mathematics

MDPI

Article

Abundant New Optical Soliton Solutions to the Biswas–Milovic Equation with Sensitivity Analysis for Optimization

Md Nur Hossain [1,2], Faisal Alsharif [3], M. Mamun Miah [4,5,*] and Mohammad Kanan [6,7,*]

[1] Graduate School of Engineering, Osaka University, Suita 565-0871, Osaka, Japan
[2] Department of Mathematics, Dhaka University of Engineering & Technology (DUET), Gazipur 1707, Bangladesh
[3] Department of Mathematics, College of Science, Taibah University, Al-Madinah Al-Munawarah 30002, Saudi Arabia
[4] Department of Mathematics, Khulna University of Engineering and Technology, Khulna 9203, Bangladesh
[5] Division of Mathematical and Physical Sciences, Kanazawa University, Kanazawa 920-1192, Ishikawa, Japan
[6] Department of Industrial Engineering, College of Engineering, University of Business and Technology, Jeddah 21448, Saudi Arabia
[7] Department of Mechanical Engineering, College of Engineering, Zarqa University, Zarqa 13110, Jordan
* Correspondence: mamun0954@stu.kanazawa-u.ac.jp (M.M.M.); m.kanan@ubt.edu.sa (M.K.)

Abstract: This study extensively explores the Biswas–Milovic equation (BME) with Kerr and power law nonlinearity to extract the unique characteristics of optical soliton solutions. These optical soliton solutions have different applications in the field of precision in optical switching, applications in waveguide design, exploration of nonlinear optical effects, imaging precision, reduced intensity fluctuations, suitability for optical signal processing in optical physics, etc. Through the powerful $(G'/G, 1/G)$-expansion analytical method, a variety of soliton solutions are expressed in three distinct forms: trigonometric, hyperbolic, and rational expressions. Rigorous validation using Mathematica software ensures precision, while dynamic visual representations vividly portray various soliton patterns such as kink, anti-kink, singular soliton, hyperbolic, dark soliton, and periodic bright soliton solutions. Indeed, a sensitivity analysis was conducted to assess how changes in parameters affect the exact solutions, aiding in the understanding of system behavior and informing decision-making, especially in accurately designing or analyzing real-world optical phenomena. This investigation reveals the significant influence of parameters λ, τ, c, $\mathcal{B}$, and K on the precise solutions in Kerr and power law nonlinearities within the BME. Notably, parameter λ exhibits consistently high sensitivity across all scenarios, while parameters τ and c demonstrate pronounced sensitivity in scenario III. The outcomes derived from this method are distinctive and carry significant implications for the dynamics of optical fibers and wave phenomena across various optical systems.

Keywords: $(G'/G, 1/G)$-expansion method; exact solutions; Biswas–Milovic equation; Kerr and power law nonlinearity; optical soliton solutions; sensitivity analysis

MSC: 35C07; 35G20; 35C08; 49Q12

Citation: Hossain, M.N.; Alsharif, F.; Miah, M.M.; Kanan, M. Abundant New Optical Soliton Solutions to the Biswas–Milovic Equation with Sensitivity Analysis for Optimization. *Mathematics* **2024**, *12*, 1585. https://doi.org/10.3390/math12101585

Academic Editors: Ben Muatjetjeja, Abdullahi Adem and P. Kaelo

Received: 26 April 2024
Revised: 10 May 2024
Accepted: 17 May 2024
Published: 19 May 2024

1. Introduction

Nonlinear equations (NLEs) are not just mathematical puzzles; instead, they are the hidden language of nature's most captivating phenomena. Unlike the straightforward lines of linear equations, NLEs capture the intricate dances of heat flow, light waves, and more, revealing the true complexity of our world. These equations unlock the secrets of solitons, solitary waves that travel through optical fibers, and hold the key to unraveling countless scientific mysteries. From the scorching heat of a furnace to the shimmering ripples of light pulses, NLEs provide a powerful lens to understand and harness these phenomena.

By deciphering their stories, mathematicians and engineers can build better fiber optic networks, design efficient heat transfer systems, and unlock the mysteries beyond the realm of light, shaping the future in remarkable ways. Furthermore, understanding and controlling soliton dynamics are crucial for various optical applications, encompassing optical communication, nonlinear optics, and ultrafast photonics. Optical solitons offer unique benefits, such as stable propagation over long distances and the preservation of pulse shape and integrity. As a result, accurate modeling of soliton dynamics is of paramount importance for advancing and optimizing optical devices and systems tailored for these specific applications [1–4]. Within the realm of optical fiber communication, the significance of the BME is notable, as it stands as a valuable tool for modeling diverse soliton solutions. These solitons represent solitary waves capable of traversing long distances without altering their form, a characteristic crucial for transmitting information without distortion [5,6]. Furthermore, their equations are integrable, indicating that they harbor an infinite number of conservation laws. This investigation delves into the interaction between parabolic and power law nonlinearities within the framework of the BME. Here is the form of the BME [5]:

$$i(\mathcal{M}^n)_t - \left\{\left(\mathcal{B}\mathbb{C}|\mathcal{M}|^2\right) - \tau\right\}\mathcal{M}^n - \mathrm{K}\left\{(\mathcal{M}^n)_{xx} + (\mathcal{M}^n)_{yy}\right\} = 0; \quad i^2 = -1. \tag{1}$$

where $\mathcal{M} = \mathcal{M}(x, y, t)$ correspond to the complex function, and $(\mathcal{M}^n)_t = \frac{\partial \mathcal{M}^n}{\partial t}$, $(\mathcal{M}^n)_{xx} = \frac{\partial^2 \mathcal{M}^n}{\partial x^2}$ and $(\mathcal{M}^n)_{yy} = \frac{\partial^2 \mathcal{M}^n}{\partial y^2}$. In Equation (1), there are three components: the first signifies the overall evolution, the second term encapsulates the function $\mathbb{C}$, representing the nonlinearity, and the third term encompasses the group velocity dispersion. Also, $\mathbb{C}$ is a real-valued algebraic function, and n serves as a constraint that extends from the nonlinear Schrödinger equation (NLSE) to the BME. The variables x, y, and t are independent spatial and temporal variables, while $\mathcal{B}$, K, and τ are real quantities.

Generally, n is larger than or equal to 1, and once n equals 1, Equation (1) shortens to the (2 + 1)-dimensional NLSE structure of the BME. This investigation centers on Equation (1), which shows evident nonlinearity, with the hypothesis that n corresponds 1 is a basic NLSE form for optical systems, particularly optical fibers.

Numerous researchers have developed various methodologies to derive precise solutions for NLSEs, employing diverse approaches such as the $\frac{G'}{G'+G+A}$ method [7,8], the Sardar subequation method [9,10], the Riccati equation method [11,12], the Hirota bilinear method [13,14], the Lie group method [15,16], the (G'/G)-expansion technique [17,18], the extended Jacobi elliptic function method [19,20], the functional variable technique [21,22], the homogeneous balance method [23,24], the Hirota bilinear formulation with N- soliton [25,26], the new auxiliary equation method [27,28], the tanh–function method [29–31], the tanh–coth method [32,33], the generalized Kudryshov method [34,35], the $\exp(-\varphi(\xi))$ - expansion method [36,37], the unified method [38,39], the multiple exp-function method [40,41] and so on.

Among various methods, the $\left(\frac{G'}{G}, \frac{1}{G}\right)$ -expansion method is a powerful analytical technique utilized in solving NLEs. It involves representing solutions as power series, where coefficients are figured out using two variables $\frac{G'}{G}$ and $\frac{1}{G}$. These coefficients are obtained by substituting the series into the equation and matching coefficients of similar terms. This method is widely employed to reveal optical solutions effectively. Numerous researchers [42–49] have utilized this technique to reveal solutions for various NLEs. Throughout history, researchers have applied diverse mathematical models like the parabolic law, Kerr law, power law, and Kudryashov's quintuple power law to probe optical soliton solutions within the framework of the BME equation, employing various solving techniques. While earlier investigations primarily centered on revealing bright and dark soliton solutions, our study takes a different approach, aiming to investigate a wider array of soliton patterns. This includes kink, anti-kink, singular soliton, hyperbolic, dark soliton, and periodic bright soliton patterns. As of present, there has been no investigation of BME employing this technique with Kerr law and power law nonlinearity. This

investigation aims to use the above-mentioned methodology to derive soliton solutions for the provided nonlinear equations. In addition to our primary investigation, we embarked on a comprehensive first-order sensitivity analysis, colloquially termed local sensitivity analysis. This analysis aims to elucidate the nuanced impacts of minor perturbations in each input parameter on the resultant outcomes within a specific operational context. This analytical endeavor involves the meticulous computation of sensitivities about the output concerning each input parameter, employing numerical methodologies such as finite differences. By scrutinizing these sensitivities, we tried to unveil the intricate interplay between individual input parameters and their consequential effects on the overarching solutions. Such insights are pivotal in augmenting our understanding of the complex dynamics of the BME's exact solutions. This paper is divided into several sections: (i) Methodology overview in Section 2. (ii) Discussion of parabolic and power law nonlinearity in Section 3. (iii) Application of the methodology to derive solutions from the equations in Section 4. (iv) Exploration of dynamic representations, showcasing soliton behaviors through 3D graphs, 2D graphs, and contours, along with sensitivity analysis of obtained solutions in Section 5. (v) Concluding remarks in Section 6. (vi) Finally, a list of relevant references.

2. A Short Overview of $(G'/G, 1/G)$-Expansion Technique

Here, we provide an in-depth explanation of the basic steps required to apply the $(G'/G, 1/G)$ technique, which was first suggested by [50], to the analysis of NLEs. To aid in this analytical process, a careful formulation of an auxiliary linear ordinary differential equation of the following form is required:

$$G''(\varphi) + \lambda G(\varphi) = \eta, \tag{2}$$

where $''$ denotes first derivatives concerning φ, and the variables are:

$$\left.\begin{array}{c} \mathcal{g} = \frac{G'(\varphi)}{G(\varphi)} \\ \mathcal{F} = \frac{1}{G(\varphi)} \end{array}\right\}. \tag{3}$$

Equation (3) satisfies the subsequent correlations:

$$\left.\begin{array}{c} \mathcal{g}' = -\mathcal{g}^2 + \eta F - \lambda \\ \mathcal{F}' = -\mathcal{g} * F \end{array}\right\}. \tag{4}$$

The result of Equation (2) mentioned earlier fluctuates depending on λ, which falls into three separate scenarios [43,51]:

Scenario ***I***: For $\lambda > 0$.

Equation (2) gives the following form of the general solution (GS):

$$G(\varphi) = l_1 sin\left(\varphi\sqrt{\lambda}\right) + l_2 cos\left(\varphi\sqrt{\lambda}\right) + \frac{\eta}{\lambda}, \tag{5}$$

which generates:

$$\mathcal{F}^2 = \left(\frac{\mathcal{g}^2 - 2\eta\mathcal{F} + \lambda}{A_1\lambda^2 - \eta^2}\right)\lambda, \tag{6}$$

where $A_1 = l_1^2 + l_2^2$ is the arbitrary constant.

Scenario II: For $\lambda < 0$

Equation (2) yields the succeeding form of the GS:

$$G(\varphi) = l_1 sinh\left(\varphi\sqrt{-\lambda}\right) + l_2 cosh\left(\varphi\sqrt{-\lambda}\right) + \frac{\eta}{\lambda}, \tag{7}$$

subsequent in:

$$\mathcal{F}^2 = -\lambda\left(\frac{\mathcal{g}^2 - 2\eta\mathcal{F} + \lambda}{A_2\lambda^2 + \eta^2}\right), \tag{8}$$

where $A_2 = l_1^2 - l_2^2$ is the arbitrary constant.

Scenario III: For $\lambda = 0$

Equation (2) results in the following form of the GS:

$$G(\varphi) = \frac{\eta\varphi^2}{2} + l_1\varphi + l_2, \tag{9}$$

which gives:

$$\mathcal{F}^2 = \left(\frac{\mathcal{g}^2 - 2\eta\mathcal{F}}{l_1^2 - 2\eta l_2}\right), \tag{10}$$

where l_1 and l_2 are the arbitrary constant.

Consider a general form of NLEs incorporating three independent variables (x, y, and t) as follows:

$$L\left(\mathcal{M}, \mathcal{M}_x, \mathcal{M}_{xx}, \mathcal{M}_y, \mathcal{M}_{yy}, \mathcal{M}_{xy}, \mathcal{M}_t, \mathcal{M}_{tt}, \mathcal{M}_{xt}, \mathcal{M}_{yt}\right) = 0, \tag{11}$$

where L denotes a polynomial function reliant on the variables encompassed in $\mathcal{M}$ and $\mathcal{M}_x = \frac{\partial\mathcal{M}}{\partial x}$, $\mathcal{M}_y = \frac{\partial\mathcal{M}}{\partial y}$, $\mathcal{M}_t = \frac{\partial\mathcal{M}}{\partial t}$, $\mathcal{M}_{xx} = \frac{\partial^2\mathcal{M}}{\partial x^2}$, $\mathcal{M}_{yy} = \frac{\partial^2\mathcal{M}}{\partial y^2}$, $\mathcal{M}_{tt} = \frac{\partial^2\mathcal{M}}{\partial t^2}$, $\mathcal{M}_{xt} = \frac{\partial\mathcal{M}}{\partial x\partial t}$, $\mathcal{M}_{xy} = \frac{\partial\mathcal{M}}{\partial x\partial y}$ and so on.

To transform Equation (11), a new variable φ is introduced, governed by the following relation:

$$\mathcal{M}(x, y, t) = e^{i\theta}\mathbb{Z}(\varphi), \tag{12}$$

where $\theta = x + y + \nu t + \sigma_0$ and $\varphi = cx + dy + \varpi t$.

Equation (12) portrays a wave characterized by a velocity of ϖ, phase described by θ, and a fixed starting point defined by the phase constant σ_0. However, to completely grasp its behavior, three real values, c, d, and ν, remain unresolved and require determination.

Now, Equation (11) is converted by using the transformation written in Equation (12) to a new form as follows:

$$J\left(\mathbb{Z}, \mathbb{Z}', \mathbb{Z}'', \mathbb{Z}''', \ldots\ldots\ldots\right) = 0. \tag{13}$$

In this context, J is the new polynomial encapsulating $\mathbb{Z}$ along with its ordinary derivatives.

The GS of Equation (13) is provided by the following equation, derived through the previously discussed method as follows:

$$\mathbb{Z}(\varphi) = a_0 + \sum_{i=1}^{N} a_i\mathcal{g}^i(\varphi) + \sum_{i=1}^{N} b_i\mathcal{g}^{i-1}(\varphi)\mathcal{F}(\varphi). \tag{14}$$

Here, a_0, a_i, and $b_i (i = 1, 2, 3, \ldots\ldots\ldots, N)$ are the arbitrary constant fulfilling the requirement $a_N^2 + b_N^2 \neq 0$, and the parameter N is defined as a positive balance number.

Exact Solution Computation Workflow:

First, applying the homogeneous balance principle to the transformed ODE provides the value of the balance number, then switching the value of N into Equation (14) and integrating the modified equation into Equation (13), with the utilization of Equations (6), (8) and (10), the left-hand side of Equation (13) transforms a polynomial containing the terms $\mathcal{g}$ and $\mathcal{F}$. In this polynomial, the degree accompanying $\mathcal{F}$ does not exceed 1, while the degree of $\mathcal{g}$ ranges from 0 to any integer. Establishing a system of algebraic equations involves equating the coefficients of terms with corresponding powers within the polynomial to 0, incorporating parameters such as a_i, b_i, λ, η, and others. Employing Mathematica software 14 aids in solving these algebraic equations to determine the values of these parameters.

Subsequently, these values are substituted into Equation (13), enabling the extraction of soliton solutions represented by trigonometric functions (as in Equation (5)), hyperbolic functions (as in Equation (7)), and rational functions (as in Equation (9)). Through the utilization of Equation (12), the exact solution of Equation (1) is derived, encompassing trigonometric, hyperbolic, and rational functions.

3. Implementation of Nonlinearities Laws

In this section, we analyzed Equation (1) using both the Ker and power law nonlinearity. The implementation of these laws on the BME is detailed in Sections 3.1 and 3.2 below.

3.1. Ker Law

For an exploration of Equation (1) under Kerr law nonlinearity, specifically when $\mathbb{C}(\Theta) = \Theta$ [52,53], the resulting NLSE is formulated as follows:

$$i\mathcal{M}_t - \left\{\left(\mathcal{B}|\mathcal{M}|^2\right) - \tau\right\}\mathcal{M} - K(\mathcal{M}_{xx} + \mathcal{M}_{yy}) = 0. \tag{15}$$

By inserting Equation (12) into Equation (15), we obtain the following equations from the imaginary and real components:

$$\{\varpi - 2K(c+d)\}\mathbb{Z}'(\varphi) = 0, \tag{16}$$

and

$$(\tau - c + 2K)\mathbb{Z}(\varphi) - \mathcal{B}\{\mathbb{Z}(\varphi)\}^3 - K\left(c^2 + d^2\right)\mathbb{Z}''(\varphi) = 0. \tag{17}$$

Given that $\mathbb{Z}(\varphi)$ is non-zero and shows second-order derivatives, Equation (16) imposes the following restriction on the velocity:

$$\varpi = 2(c+d)K. \tag{18}$$

Hence, Equation (17) signifies the NODE (nonlinear ordinary differential equation) form of Equation (15) with Kerr law nonlinearity, subject to the constraint outlined in Equation (18).

3.2. Power Law

In examining Equation (1) under power law nonlinearity, specifically when $\mathbb{C}(\Theta) = \Theta^n$ [52,53], the resulting NLSE is formulated as follows:

$$i\mathcal{M}_t - \left\{\left(\mathcal{B}|\mathcal{M}|^{2n}\right) - \tau\right\}\mathcal{M} - K\{\mathcal{M}_{xx} + \mathcal{M}_{yy}\} = 0. \tag{19}$$

In this scenario, for stability, it is imperative that $0 < n < 2$. By inserting Equation (12) into Equation (19) and organizing the resulting expression, the following equations are derived:

$$\{\varpi - 2K(c+d)\}\mathbb{Z}'(\varphi) = 0, \tag{20}$$

and

$$\left[-\mathcal{B}\{\mathbb{Z}(\varphi)\}^{2n} + \tau - c + 2K\right]\mathbb{Z}(\varphi) - \mathrm{K}\left(c^2 + d^2\right)\mathbb{Z}''(\varphi) = 0. \tag{21}$$

Likewise, Equation (21) offers the following restriction on the velocity:

$$\varpi = 2(c+d)K. \tag{22}$$

Therefore, Equation (21) signifies the NODE form of Equation (19) with power law nonlinearity, subject to the constraint outlined in Equation (22).

4. Method's Application with Nonlinearities Laws

In this segment, we employ the methodologies elucidated in Section 2 to derive the optical soliton solution for Equation (1).

4.1. Application for Kerr Law

Through the application of the balancing principle in Equation (17) provides $N = 1$. Therefore, Equation (14) transforms into the following form:

$$\mathbb{Z}(\varphi) = a_0 + a_1 \mathcal{g}(\varphi) + b_1 \mathcal{F}(\varphi). \tag{23}$$

In this equation, the coefficients a_0, a_1 and b_1 are constants that need to be decided.

Scenario I. $\lambda > 0$ (For trigonometric)

To obtain the solutions for Equation (17), we use Equations (4) and (6) and replace Equation (17) with Equation (23). With this technique, a polynomial with $\mathcal{g}$ and $\mathcal{F}$ is created from the left side of Equation (17). This polynomial's coefficients, a_0, a_1 and b_1, are involved in a system of algebraic equations when each coefficient is set to zero. Solving this system of algebraic equations yields the follows arbitrary constants:

$$\left.\begin{array}{c} a_0 = 0 \\ a_1 = \pm\frac{\sqrt{-(c^2+d^2)K}}{\sqrt{2}\sqrt{\mathcal{B}}} \\ b_1 = \pm\frac{\sqrt{-(c^2+d^2)K}\sqrt{\lambda^2 \mathrm{A}_1 - \eta^2}}{\sqrt{2}\sqrt{\mathcal{B}}\sqrt{\lambda}} \end{array}\right\},$$

where $\tau = \frac{1}{2}\left(2c - 4K + c^2K\lambda + d^2K\lambda\right)$ and $K < 0$.

Now, using these calculated values in Equation (14), we obtain the following solution of Equation (17):

$$\begin{array}{c} \mathbb{Z}(\varphi) = \pm\frac{\sqrt{-(c^2+d^2)K}}{\sqrt{2}\sqrt{\mathcal{B}}}\sqrt{\lambda}\frac{l_1 cos\left(\varphi\sqrt{\lambda}\right) - l_2 sin\left(\varphi\sqrt{\lambda}\right)}{l_1 sin\left(\varphi\sqrt{\lambda}\right) + l_2 cos\left(\varphi\sqrt{\lambda}\right) + \frac{\eta}{\lambda}} \pm \\ \frac{\sqrt{-(c^2+d^2)K}\sqrt{\lambda^2 A_1 - \eta^2}}{\sqrt{2}\sqrt{\mathcal{B}}\sqrt{\lambda}}\frac{1}{l_1 sin\left(\varphi\sqrt{\lambda}\right) + l_2 cos\left(\varphi\sqrt{\lambda}\right) + \frac{\eta}{\lambda}}, \end{array} \tag{24}$$

where $\varphi = cx + dy + 2(c+d)Kt$.

Reverting to its first form with the aid of Equation (12), we obtain the following form:

$$\begin{array}{c} \mathcal{M}(x,y,t) = e^{i\theta}\left\{\pm\frac{\sqrt{-(c^2+d^2)K}}{\sqrt{2}\sqrt{\mathcal{B}}}\sqrt{\lambda}\frac{l_1 cos\left(\varphi\sqrt{\lambda}\right) - l_2 sin\left(\varphi\sqrt{\lambda}\right)}{l_1 sin\left(\varphi\sqrt{\lambda}\right) + l_2 cos\left(\varphi\sqrt{\lambda}\right) + \frac{\eta}{\lambda}} \pm \right. \\ \left. \frac{\sqrt{-(c^2+d^2)K}\sqrt{\lambda^2 A_1 - \eta^2}}{\sqrt{2}\sqrt{\mathcal{B}}\sqrt{\lambda}}\frac{1}{l_1 sin\left(\varphi\sqrt{\lambda}\right) + l_2 cos\left(\varphi\sqrt{\lambda}\right) + \frac{\eta}{\lambda}}\right\}, \end{array} \tag{25}$$

where $\varphi = cx + dy + 2(c+d)Kt$ and $\theta = x + y + \nu t + \sigma_0$.

Scenario II. $\lambda < 0$ (For hyperbolic)

To derive the hyperbolic solution, apply the same procedure, resulting in:

$$\left.\begin{array}{c} a_0 = 0 \\ a_1 = \pm\frac{\sqrt{-(c^2+d^2)K}}{\sqrt{2}\sqrt{\mathcal{B}}} \\ b_1 = \pm\frac{\sqrt{-(c^2+d^2)K}\sqrt{\eta^2 + \lambda^2 \mathrm{A}_2}}{\sqrt{2}\sqrt{\mathcal{B}}\sqrt{-\lambda}} \end{array}\right\},$$

where $\tau = \frac{1}{2}\left(2c - 4K + c^2K\lambda + d^2K\lambda\right)$ and $K < 0$.

Now, using these calculated values in Equation (14), the following solution of Equation (17):

$$\mathbb{Z}(\varphi) = \pm\frac{\sqrt{-(c^2+d^2)K}}{\sqrt{2}\sqrt{\mathcal{B}}}\sqrt{-\lambda}\frac{l_1 cosh\left(\varphi\sqrt{-\lambda}\right)+l_2 sinh\left(\varphi\sqrt{-\lambda}\right)}{l_1 sinh\left(\varphi\sqrt{-\lambda}\right)+l_2 cosh\left(\varphi\sqrt{-\lambda}\right)+\frac{\eta}{\lambda}} \pm \frac{\sqrt{-(c^2+d^2)K}}{\sqrt{2}\sqrt{\mathcal{B}}\sqrt{-\lambda}}\sqrt{\eta^2+\lambda^2 A_2}\frac{1}{l_1 sinh\left(\varphi\sqrt{-\lambda}\right)+l_2 cosh\left(\varphi\sqrt{-\lambda}\right)+\frac{\eta}{\lambda}}, \tag{26}$$

where $\varphi = cx + dy + 2(c+d)Kt$.

With the help of Equation (12), obtain solution of main PDEs:

$$\mathcal{M}(x,y,t) = e^{i\theta}\left\{\pm\frac{\sqrt{-(c^2+d^2)K}}{\sqrt{2}\sqrt{\mathcal{B}}}\sqrt{-\lambda}\frac{l_1 cosh\left(\varphi\sqrt{-\lambda}\right)+l_2 sinh\left(\varphi\sqrt{-\lambda}\right)}{l_1 sinh\left(\varphi\sqrt{-\lambda}\right)+l_2 cosh\left(\varphi\sqrt{-\lambda}\right)+\frac{\eta}{\lambda}} \pm \frac{\sqrt{-(c^2+d^2)K}}{\sqrt{2}\sqrt{\mathcal{B}}\sqrt{-\lambda}}\sqrt{\eta^2+\lambda^2 A_2}\frac{1}{l_1 sinh\left(\varphi\sqrt{-\lambda}\right)+l_2 cosh\left(\varphi\sqrt{-\lambda}\right)+\frac{\eta}{\lambda}}\right\} \tag{27}$$

where $\varphi = cx + dy + 2(c+d)Kt$ and $\theta = x + y + \nu t + \sigma_0$.

When l_1 is confirmed to be non-zero and both η and l_2 are set to zero, Equation (27) takes on the form of the following soliton solution:

$$\mathcal{M}(x,y,t) = e^{i\theta}\left\{\pm\frac{\sqrt{-(c^2+d^2)K}}{\sqrt{2}\sqrt{\mathcal{B}}}\sqrt{-\lambda}coth(\varphi\sqrt{-\lambda}) \pm \frac{\sqrt{-(c^2+d^2)K}}{\sqrt{2}\sqrt{\mathcal{B}}\sqrt{-\lambda}}\lambda cosech(\varphi\sqrt{-\lambda})\right\}, \tag{28}$$

where $\varphi = cx + dy + 2(c+d)Kt$ and $\theta = x + y + \nu t + \sigma_0$.

Scenario III. For $\lambda = 0$ (For rational)

To achieve the rational solution, follow the same procedure outlined in scenario I, resulting in:

$$\left.\begin{array}{c} a_0 = 0 \\ a_1 = \pm\frac{\sqrt{c^2+d^2}\sqrt{\tau-c}}{2\sqrt{\mathcal{B}}} \\ b_1 = \pm\frac{\sqrt{c^2+d^2}\sqrt{\tau-c}\sqrt{l_1^2-2l_2\eta}}{2\sqrt{\mathcal{B}}} \end{array}\right\},$$

where $K = \frac{c-\tau}{2}$.

Now, incorporating these computed values into Equation (14), we derive the following solution for Equation (17):

$$\mathbb{Z}(\varphi) = \pm\frac{\sqrt{c^2+d^2}\sqrt{\tau-c}}{2\sqrt{\mathcal{B}}}\frac{2\eta\varphi + l_1}{\frac{\eta}{2}\varphi^2 + l_1\varphi + l_2} \pm \frac{\sqrt{c^2+d^2}\sqrt{\tau-c}\sqrt{l_1^2-2l_2\eta}}{2\sqrt{\mathcal{B}}}\frac{1}{\frac{\eta}{2}\varphi^2 + l_1\varphi + l_2}, \tag{29}$$

where $\varphi = cx + dy + 2(c+d)Kt$.

Inserting the transformation variables defined in Equation (12) into the above equation results in the following generalized solution for Equation (1):

$$\mathcal{M}(x,y,t) = e^{i\theta}\left\{\pm\frac{\sqrt{c^2+d^2}\sqrt{\tau-c}}{2\sqrt{\mathcal{B}}}\frac{2\eta\varphi + l_1}{\frac{\eta}{2}\varphi^2 + l_1\varphi + l_2} \pm \frac{\sqrt{c^2+d^2}\sqrt{\tau-c}\sqrt{l_1^2-2l_2\eta}}{2\sqrt{\mathcal{B}}}\frac{1}{\frac{\eta}{2}\varphi^2 + l_1\varphi + l_2}\right\}, \tag{30}$$

where $\varphi = cx + dy + 2(c+d)Kt$ and $\theta = x + y + \nu t + \sigma_0$.

When l_1 is confirmed to be non-zero and both η and l_2 are set to zero, Equation (30) takes on the form of the following soliton solution:

$$\mathcal{M}(x,y,t) = e^{i\theta}\left\{\pm\frac{\sqrt{c^2+d^2}\sqrt{\tau-c}}{2\sqrt{\mathcal{B}}}\frac{1}{\varphi} \pm \frac{\sqrt{c^2+d^2}\sqrt{\tau-c}}{2\sqrt{\mathcal{B}}}\frac{1}{\varphi}\right\}, \tag{31}$$

where $\varphi = cx + dy + 2(c+d)Kt$ and $\theta = x + y + \nu t + \sigma_0$.

4.2. Application for Power Law

Operating the balancing principle in Equation (21), we deduce that $N = 1/n$. Consequently, the following relation can be defined:

$$\mathbb{Z}(\varphi) = \Upsilon(\varphi)^{\frac{1}{n}}. \tag{32}$$

Thus, employing the transformation, Equation (38) undergoes the following form:

$$(\tau - c + 2K)n^2\{Y(\varphi)\}^2 - \mathcal{B}n^2\{Y(\varphi)\}^4 + K\left(c^2 + d^2\right)(n-1)\{Y'(\varphi)\}^2 - nK\left(c^2 + d^2\right)Y(\varphi)Y''(\varphi) = 0. \tag{33}$$

Applying the balancing principle once more and figuring out $N = 1$, the solution adopts the following structure:

$$Y(\varphi) = a_0 + a_1\mathcal{G}(\varphi) + b_1\mathcal{F}(\varphi). \tag{34}$$

Now, employing a similar procedure as described in Section 4.1 for all scenarios, we derive the following solutions for Equation (33), then Equation (21), and finally Equation (1):

Scenario I. $\lambda > 0$ (For trigonometric)

The coefficients obtained from this case are as follows:

$$\left.\begin{array}{c} a_0 = 0 \\ a_1 = \pm\frac{\sqrt{c-\tau-2K}}{\sqrt{\mathcal{B}}\sqrt{\lambda}} \\ b_1 = \pm\frac{\sqrt{c-\tau-2K}\sqrt{\lambda^2A_1-\eta^2}}{\sqrt{\mathcal{B}}\lambda} \end{array}\right\},$$

where $d = \pm\frac{\sqrt{2c-2\tau-4K+c^2K\lambda}\sqrt{\lambda^2A_1-\eta^2}}{\sqrt{\lambda}\sqrt{K\eta^2-K\lambda^2A_1}}$ and $n = 1$.

Now, utilizing these computed values in Equation (34), we derive the following solution for Equation (33):

$$\begin{array}{c} Y(\varphi) = \pm\frac{\sqrt{c-\tau-2K}}{\sqrt{\mathcal{B}}\sqrt{\lambda}}\sqrt{\lambda}\frac{l_1cos\left(\varphi\sqrt{\lambda}\right)-l_2sin\left(\varphi\sqrt{\lambda}\right)}{l_1sin\left(\varphi\sqrt{\lambda}\right)+l_2cos\left(\varphi\sqrt{\lambda}\right)+\frac{\eta}{\lambda}}\pm \\ \frac{\sqrt{c-\tau-2K}\sqrt{\lambda^2A_1-\eta^2}}{\sqrt{\mathcal{B}}\lambda}\frac{1}{l_1sin\left(\varphi\sqrt{\lambda}\right)+l_2cos\left(\varphi\sqrt{\lambda}\right)+\frac{\eta}{\lambda}}, \end{array} \tag{35}$$

where $\varphi = cx + dy + 2(c+d)Kt$.

Returning to its original form with the aid of Equation (12), we obtain the following equation:

$$\begin{array}{c} \mathcal{M}(x,y,t) = e^{i\theta}\left\{\pm\frac{\sqrt{c-\tau-2K}}{\sqrt{\mathcal{B}}}\frac{l_1cos\left(\varphi\sqrt{\lambda}\right)-l_2sin\left(\varphi\sqrt{\lambda}\right)}{l_1sin\left(\varphi\sqrt{\lambda}\right)+l_2cos\left(\varphi\sqrt{\lambda}\right)+\frac{\eta}{\lambda}}\pm\right. \\ \left.\frac{\sqrt{c-\tau-2K}\sqrt{\lambda^2A_1-\eta^2}}{\sqrt{\mathcal{B}}\lambda}\frac{1}{l_1sin\left(\varphi\sqrt{\lambda}\right)+l_2cos\left(\varphi\sqrt{\lambda}\right)+\frac{\eta}{\lambda}}\right\}, \end{array} \tag{36}$$

where $\varphi = cx + dy + 2(c+d)Kt$ and $\theta = x + y + \nu t + \sigma_0$.

When l_2 is confirmed to be non-zero and both η and l_1 are set to zero, Equation (36) takes on the form of the following soliton solution:

$$\mathcal{M}(x,y,t) = e^{i\theta}\left\{\pm\frac{\sqrt{c-\tau-2K}}{\sqrt{\mathcal{B}}}tan\left(\varphi\sqrt{\lambda}\right) \pm \frac{\sqrt{c-\tau-2K}}{\sqrt{\mathcal{B}}}sec\left(\varphi\sqrt{\lambda}\right)\right\}, \tag{37}$$

where $\varphi = cx + dy + 2(c+d)Kt$ and $\theta = x + y + \nu t + \sigma_0$.

When l_1 is confirmed to be non-zero and both η and l_2 are set to zero, Equation (36) takes on the form of the following soliton solution:

$$\mathcal{M}(x,y,t) = e^{i\theta}\left\{\pm\frac{\sqrt{c-\tau-2K}}{\sqrt{\mathcal{B}}}cot\left(\varphi\sqrt{\lambda}\right) \pm \frac{\sqrt{c-\tau-2K}}{\sqrt{\mathcal{B}}}cosec\left(\varphi\sqrt{\lambda}\right)\right\}, \quad (38)$$

where $\varphi = cx + dy + 2(c+d)Kt$ and $\theta = x + y + \nu t + \sigma_0$.

Scenario II. When $\lambda < 0$ (For hyperbolic)

The obtained coefficients for this case are as follows:

$$\left.\begin{array}{c} a_0 = 0 \\ a_1 = \pm\frac{\sqrt{\tau+2K-c}}{\sqrt{\mathcal{B}}\sqrt{-\lambda}} \\ b_1 = \pm\frac{\sqrt{\tau+2K-c}\sqrt{\lambda^2 A_2+\eta^2}}{\sqrt{\mathcal{B}}\lambda} \end{array}\right\},$$

where $d = \pm\frac{\sqrt{2c-2\tau-4K+c^2K\lambda}\sqrt{\lambda^2 A_1+\eta^2}}{\sqrt{-\lambda}\sqrt{K\eta^2+K\lambda^2 A_2}}$ and $n = 1$.

Now, incorporating these calculated values into Equation (34), we derive the following solution for Equation (33):

$$\begin{array}{c} Y(\varphi) = \pm\frac{\sqrt{\tau+2K-c}}{\sqrt{\mathcal{B}}\sqrt{-\lambda}}\sqrt{-\lambda}\frac{l_1 cosh\left(\varphi\sqrt{-\lambda}\right)+l_2 sinh\left(\varphi\sqrt{-\lambda}\right)}{l_1 sinh\left(\varphi\sqrt{-\lambda}\right)+l_2 cosh\left(\varphi\sqrt{-\lambda}\right)+\frac{\eta}{\lambda}} \pm \\ \frac{\sqrt{\tau+2K-c}\sqrt{\lambda^2 A_2+\eta^2}}{\sqrt{\mathcal{B}}\lambda}\frac{1}{l_1 sinh\left(\varphi\sqrt{-\lambda}\right)+l_2 cosh\left(\varphi\sqrt{-\lambda}\right)+\frac{\eta}{\lambda}}, \end{array} \quad (39)$$

where $\varphi = cx + dy + 2(c+d)Kt$.

Returning to its original form with the aid of Equation (12), we obtain the following equation:

$$\begin{array}{c} \mathcal{M}(x,y,t) = e^{i\theta}\left\{\pm\frac{\sqrt{\tau+2K-c}}{\sqrt{\mathcal{B}}}\frac{l_1 cosh\left(\varphi\sqrt{-\lambda}\right)+l_2 sinh\left(\varphi\sqrt{-\lambda}\right)}{l_1 sinh\left(\varphi\sqrt{-\lambda}\right)+l_2 cosh\left(\varphi\sqrt{-\lambda}\right)+\frac{\eta}{\lambda}} \pm\right. \\ \left.\frac{\sqrt{\tau+2K-c}\sqrt{\lambda^2 A_2+\eta^2}}{\sqrt{\mathcal{B}}\lambda}\frac{1}{l_1 sinh\left(\varphi\sqrt{-\lambda}\right)+l_2 cosh\left(\varphi\sqrt{-\lambda}\right)+\frac{\eta}{\lambda}}\right\}, \end{array} \quad (40)$$

where $\varphi = cx + dy + 2(c+d)Kt$ and $\theta = x + y + \nu t + \sigma_0$.

When l_1 is confirmed to be non-zero and both η and l_2 are set to zero, Equation (40) takes on the form of the following soliton solution:

$$\mathcal{M}(x,y,t) = e^{i\theta}\left\{\pm\frac{\sqrt{\tau+2K-c}}{\sqrt{\mathcal{B}}}coth\left(\varphi\sqrt{-\lambda}\right) \pm \frac{\sqrt{\tau+2K-c}}{\sqrt{\mathcal{B}}}cosech\left(\varphi\sqrt{-\lambda}\right)\right\}, \quad (41)$$

where $\varphi = cx + dy + 2(c+d)Kt$ and $\theta = x + y + \nu t + \sigma_0$.

Scenario III. If $\lambda = 0$ (For rational)

The obtained coefficients for this case are as follows:

$$\left.\begin{array}{c} a_0 = 0 \\ a_1 = \pm\frac{\sqrt{c^2+d^2}\sqrt{\tau-c}\sqrt{1+n}}{2\sqrt{2}n\sqrt{\mathcal{B}}} \\ b_1 = \pm\frac{\sqrt{c^2+d^2}\sqrt{\tau-c}\sqrt{l_1^2-2l_2\eta}}{2\sqrt{2}n\sqrt{\mathcal{B}}} \end{array}\right\},$$

where $K = \frac{c-\tau}{2}$.

Now, using these calculated values in Equation (34), we obtain the following solution for Equation (33):

$$Y(\varphi) = \pm\frac{\sqrt{c^2+d^2}\sqrt{\tau-c}\sqrt{1+n}}{2\sqrt{2}n\sqrt{\mathcal{B}}}\frac{2\eta\varphi+l_1}{\frac{\eta}{2}\varphi^2+l_1\varphi+l_2} \pm \frac{\sqrt{c^2+d^2}\sqrt{\tau-c}\sqrt{l_1^2-2l_2\eta}}{2\sqrt{2}n\sqrt{\mathcal{B}}}\frac{1}{\frac{\eta}{2}\varphi^2+l_1\varphi+l_2}, \quad (42)$$

where $\varphi = cx + dy + 2(c+d)Kt$.

Plugging in the transformation variables outlined in Equation (12) into the given equation produces the following comprehensive solution for Equation (1):

$$\mathcal{M}(x,y,t) = e^{i\theta}\left\{ \pm \frac{\sqrt{c^2+d^2}\sqrt{\tau-c}\sqrt{1+n}}{2\sqrt{2}n\sqrt{\mathcal{B}}} \frac{2\eta\varphi+l_1}{\frac{\eta}{2}\varphi^2+l_1\varphi+l_2} \pm \frac{\sqrt{c^2+d^2}\sqrt{\tau-c}\sqrt{l_1^2-2l_2\eta}}{2\sqrt{2}n\sqrt{\mathcal{B}}} \frac{1}{\frac{\eta}{2}\varphi^2+l_1\varphi+l_2} \right\}^{\frac{1}{n}}, \tag{43}$$

where $\varphi = cx + dy + 2(c+d)Kt$ and $\theta = x + y + \nu t + \sigma_0$.

Setting both η and l_2 to zero, while ensuring l_1 is non-zero, Equation (30) simplifies to yield the soliton solution in the following manner:

$$\mathcal{M}(x,y,t) = e^{i\theta}\left\{ \pm \frac{\sqrt{c^2+d^2}\sqrt{\tau-c}\sqrt{1+n}}{2\sqrt{2}n\sqrt{\mathcal{B}}} \frac{1}{\varphi} \pm \frac{\sqrt{c^2+d^2}\sqrt{\tau-c}}{2\sqrt{2}n\sqrt{\mathcal{B}}} \frac{1}{\varphi} \right\}^{\frac{1}{n}}, \tag{44}$$

where $\varphi = cx + dy + 2(c+d)Kt$ and $\theta = x + y + \nu t + \sigma_0$.

5. Graphs and Meanings

Harnessing the power of Mathematica, an advanced mathematical computing tool, we explored the intricate graphical patterns shown by the BME with Kerr law nonlinearity and BME with Power law nonlinearity. Our presentation encompasses a variety of visual representations, including 3D renderings, 2D graphical displays, and contour plots. These visualizations cover a broad range of parameter values for each relevant variable, allowing us to gain a thorough insight into the graphical behavior of these nonlinear equations across diverse parameter space.

To ensure clarity and conciseness, we opted for three representative solution sets for each case (BME with Kerr law nonlinearity and BME with power law nonlinearity) from our comprehensive results for visual representation, standardizing only three graphs, including 3D renderings, 2D graphical displays, and contour plots, for each nonlinearity. The specific constants linked to each graph are detailed in the corresponding figure captions. In 2D graphs, we consolidated multiple solutions within a single figure by varying the parameter t.

5.1. Visualization of the BME with Kerr Law Nonlinearity

The depiction in Figure 1, originating from Equation (25), vividly captures the essence of periodic bright solitons. These solitons, known for their periodic behavior and stable propagation, hold immense utility across various domains such as optical communications, nonlinear optics, and fiber optics. Their unique ability to convey information over extended distances without distortion is highly advantageous. Moreover, they serve as invaluable tools for studying wave dynamics and nonlinear phenomena, shedding light on the intricate behavior of light pulses within optical fibers and other waveguides.

The image portrayed in Figure 2, stemming from Equation (28), vividly illustrates the essence of kink-type solitons with singular characteristics. These solitons are recognized by their localized wave packets with a kink-shaped profile, showcasing distinctive behavior during optical fiber propagation. Renowned for their singular attributes, they hold significance across diverse optical fiber applications, spanning signal processing, nonlinear optics, and optical communications. Their exceptional features make them invaluable for enhancing the stability and efficiency of optical signal manipulation and transmission within fiber optic networks.

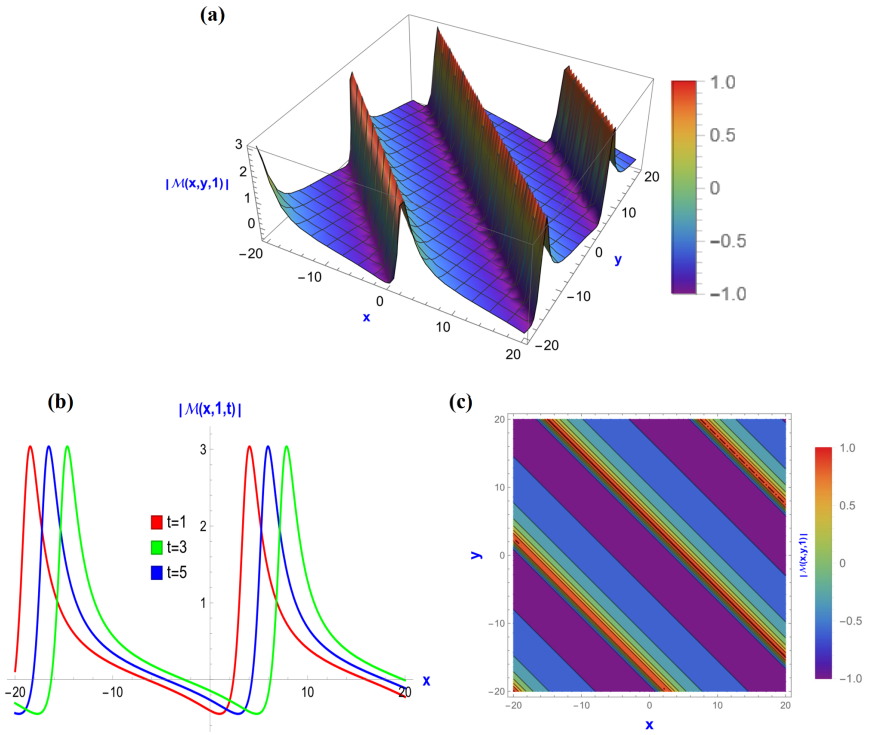

Figure 1. Graphs of the solution $|\mathcal{M}(x,y,t)|$ of Equation (25) for $\lambda = 1.95, \mathrm{K} = -3.05$, $\mathcal{B} = 2.6$, $\eta = 2.9$, $c = 0.2$, $d = 0.2$, $l_1 = 1.2$ and $l_2 = 0.75$**:** (**a**) A three-dimensional visualization showcasing the periodic bright soliton, (**b**) a two-dimensional visualization showcasing the periodic bright soliton, and (**c**) a contour depiction of periodic bright soliton.

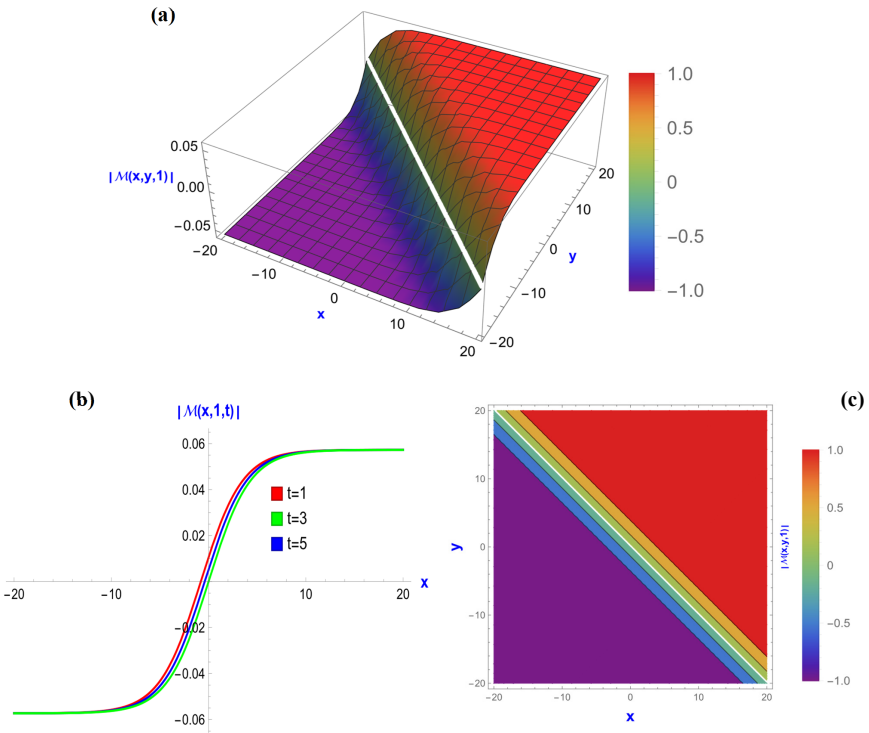

Figure 2. Graphs of the solution $|\mathcal{M}(x,y,t)|$ of Equation (28) for $\lambda = -5.5, \mathrm{K} = -0.05$, $\mathcal{B} = 3.35$, $\eta = 0.2$, $c = 0.2$, $d = 0.2$, $l_1 = 0.1$ and $l_2 = -3.41$: (**a**) A 3D depiction of kink-type soliton solution, (**b**) a 2D illustration of kink-type soliton solution, and (**c**) a contour portrayal of kink-type soliton solution.

Figure 3, originating from Equation (30), showcases dark-type solitons. These solitons, characterized by localized waveforms with reduced intensities, are essential for various optical communication tasks such as signal amplification, pulse compression, and signal regeneration within fiber optic networks. Their unique ability to keep waveform integrity during propagation through optical fibers ensures reliable and efficient data transmission over long distances in optical communication systems. Geometrically, a dark soliton is a depressed section within a wave, where the amplitude falls below the neighboring crests, creating a noticeable trough. This imagery mirrors a dim, less intense area amid the brighter wave peaks, showcasing the soliton's unique trait of maintaining its shape and conserving energy while moving through the medium.

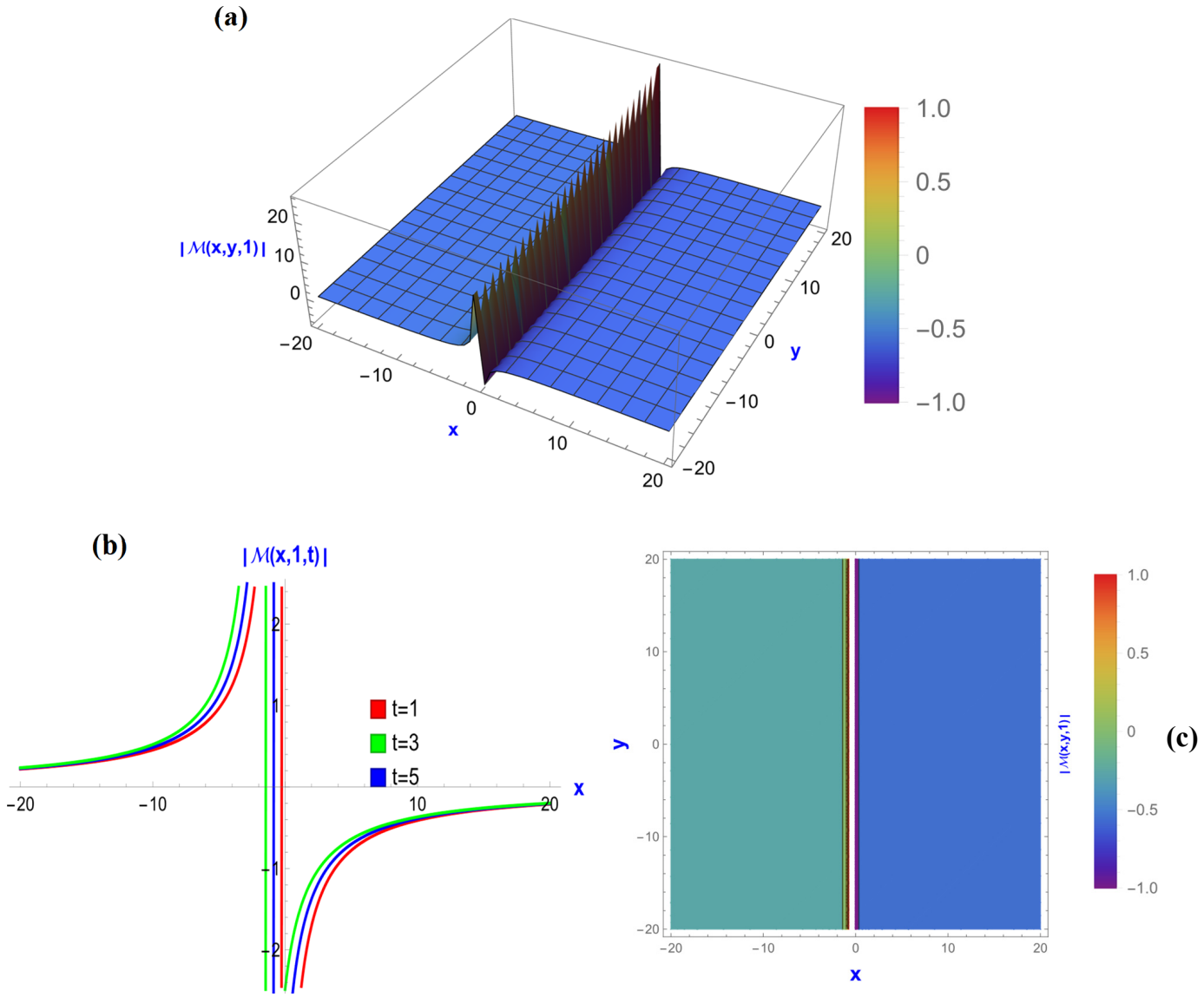

Figure 3. Graphs of the solution $|\mathcal{M}(x,y,t)|$ of Equation (30) for K $= 0.25$, $\mathcal{B} = 1.1$, $\eta = -5.02$, $c = -0.01$, $d = -5.1$, $l_1 = 0.5$ and $l_2 = 0.02$: (**a**) A 3D representation of dark-type soliton, (**b**) a 2D representation of dark-type soliton, and (**c**) a contour representation of dark-type soliton.

5.2. Sensitivity Analysis

Sensitivity analysis involves scrutinizing how variations in input parameters impact the output of a model or system within a localized region of the parameter space. In recent studies, researchers [54,55] have utilized this analysis to explore how adjustments in input parameters influence the output of NLEs. In this section, we conduct a local sensitivity

analysis of our derived solution for each scenario (for $\lambda = 0,\ \lambda < 0$, and $\lambda > 0$). Figure 4a illustrates the sensitivity of each parameter in Equation (25) for Scenario I. We note that parameters $(\lambda,\ c,\ d,\ l_1,\ \mathrm{K})$ show negative sensitivity, whereas λ demonstrates notably high negative sensitivity. On the other hand, the remaining parameters $(\mathcal{B}, \eta,\ l_2)$ exhibit positive sensitivity, although not as pronounced as λ. Additionally, it is apparent that l_2 exhibits almost negligible sensitivity compared to others. For Scenario II ($\lambda < 0$), the results remain largely consistent, with one notable difference: the parameter K shows slightly higher sensitivity compared to λ, as depicted in Figure 4b. In the case of a rational solution ($\lambda = 0$), the most sensitive parameters are c and τ, but they exhibit opposite directions of sensitivity, whereas other parameters are nearly negligible, as illustrated in Figure 4c.

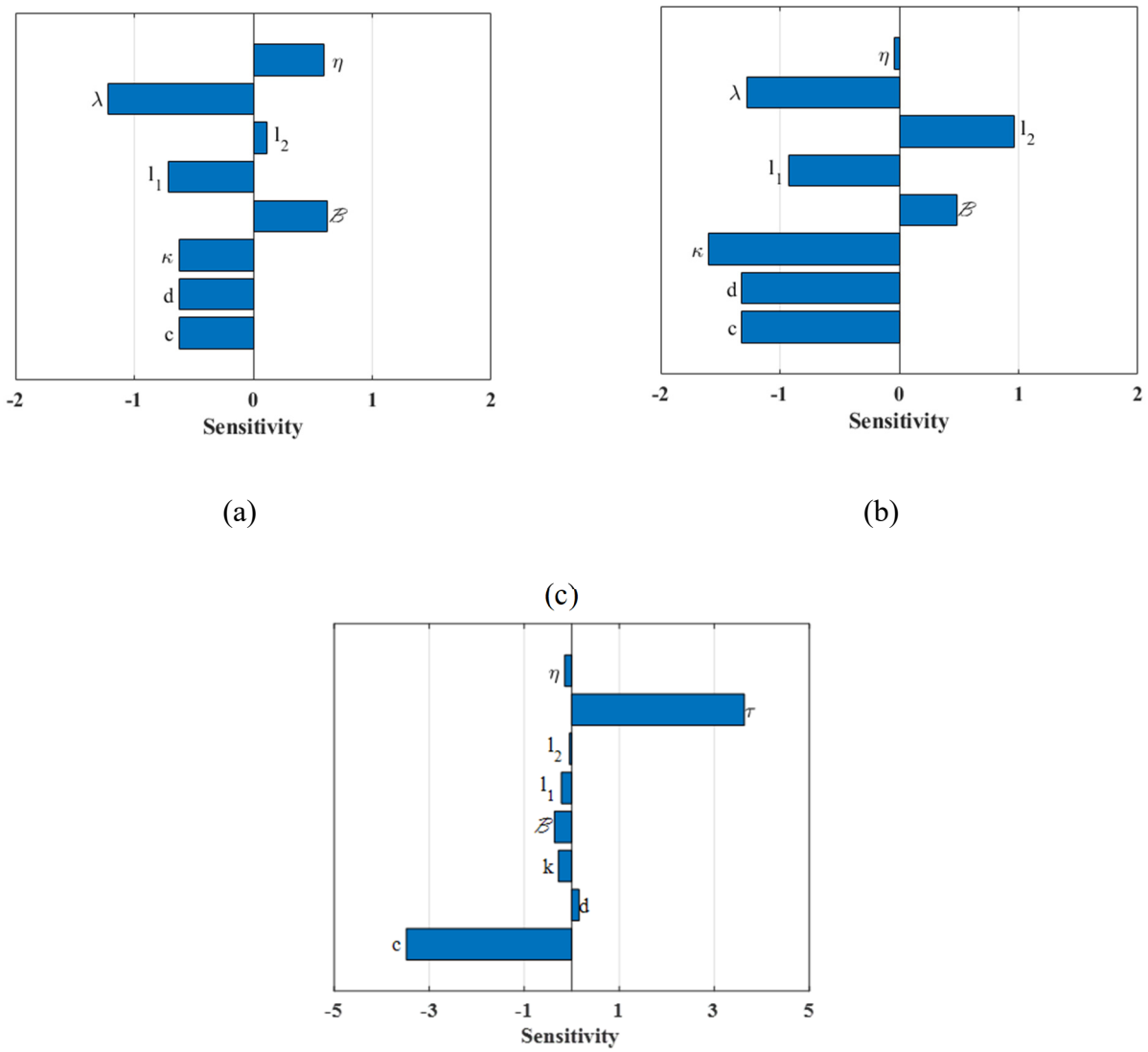

Figure 4. Sensitivity analysis:(**a**) $\lambda > 0$ for Equation (25), (**b**) $\lambda < 0$ for Equation (27), and (**c**) $\lambda = 0$, for Equation (30).

5.3. The Graphical Representation of the BME with Power Law Nonlinearity

Figure 5, originating from Equation (38), depicts a singular soliton type. This variant of solitons within optical fibers enables the transmission of information over extensive distances with minimal distortion, representing notable advancements in telecommunications and optical signal processing. Renowned for their ability to preserve shape and velocity during propagation, these solitary waves play a critical role in elevating data transmission rates and mitigating signal degradation in fiber optic communication systems.

The anti-kink soliton solution, derived from Equation (40) and depicted in Figure 6, is vital in optical fibers. It effectively counters kinks or distortions, preserving signal integrity and ensuring reliable long-distance communication. This is crucial in high-speed networks and fiber optic systems where signal degradation is detrimental. Additionally, anti-kink solitons enhance overall efficiency and stability, supporting the advancement of optical fiber-based technologies and high-capacity data transmission networks.

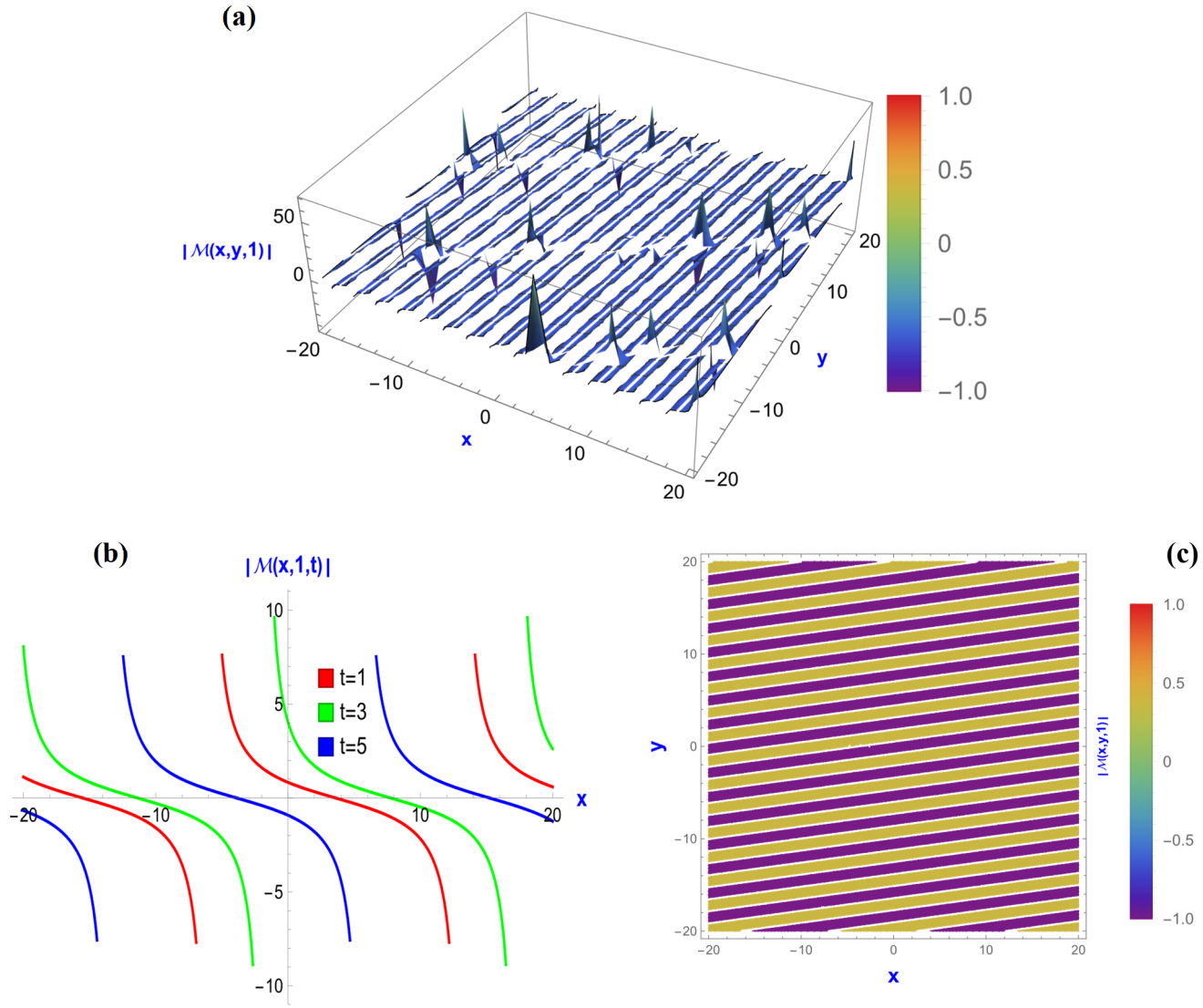

Figure 5. Graphical representations of the solutions $|\mathcal{M}(x,y,t)|$ of Equation (38) for $\lambda = 1.2$, $K = -1.05$, $\mathcal{B} = 1.5$, $c = 0.3$, $d = -2.2$, $\tau = 0.1$, $l_1 = 0.2$ and $l_2 = -0.75$: (**a**) A 3D depiction of singular soliton, (**b**) a 2D depiction of singular soliton, and (**c**) contour interpretation of singular soliton.

The solution derived from Equation (43) and illustrated in Figure 7 is of the hyperbolic type. Within optical fibers, this type of solution ensures stable signal transmission by preserving shape and velocity, minimizing distortion across long distances. Offering high energy and bandwidth, hyperbolic solutions facilitate efficient signal amplification and support high-capacity data transmission. Their robust characteristics enable extended transmission distances and improved signal quality. Moreover, hyperbolic solitons enable nonlinear effects such as soliton self-frequency shifting and supercontinuum generation, broadening their applications in nonlinear optics and photonics. Overall, they significantly elevate the performance and capabilities of optical fiber communication networks.

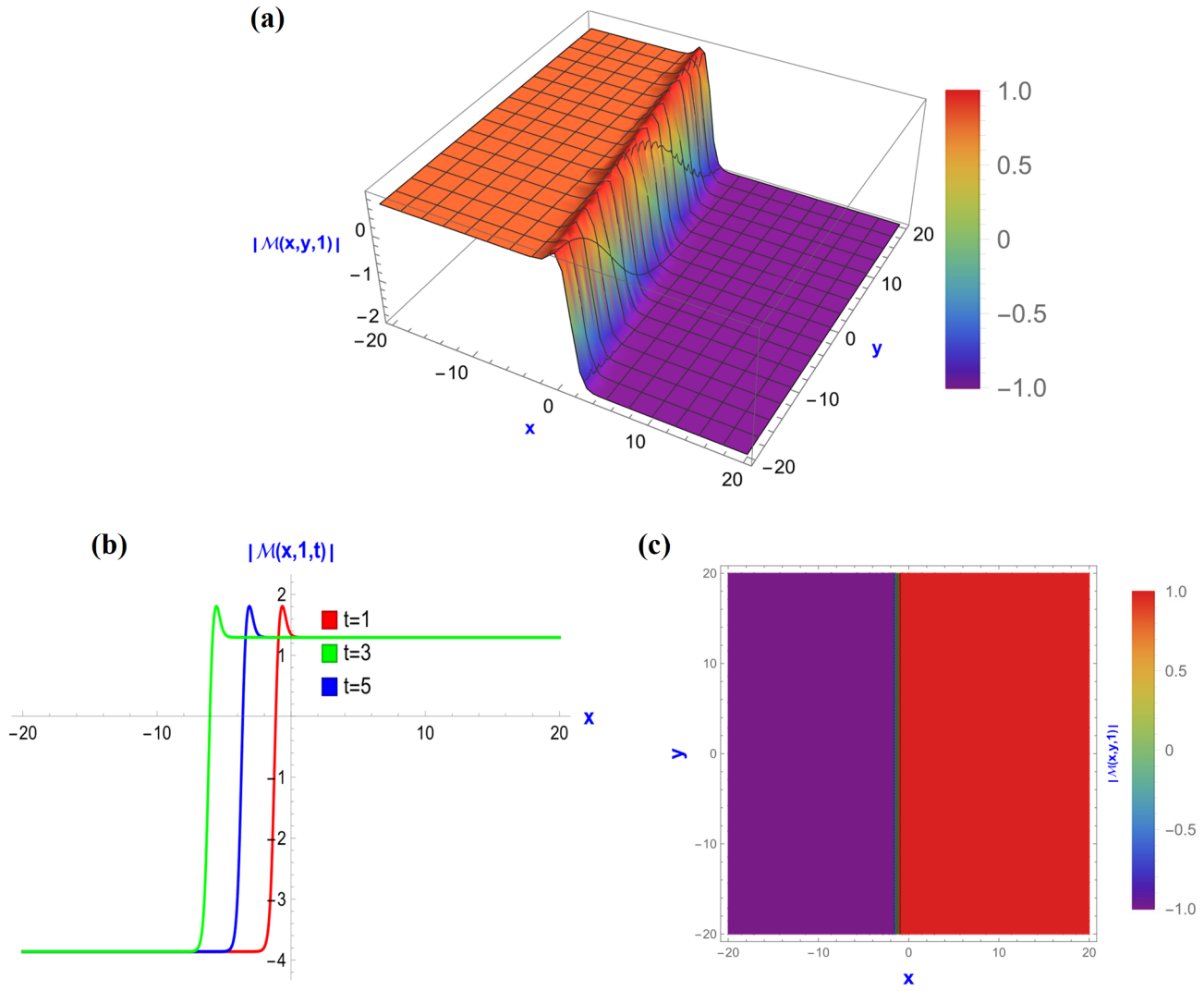

Figure 6. Graphs of the solution $|\mathcal{M}(x,y,t)|$ of Equation (40) for $\lambda = -1.2, \mathrm{K} = 1.05$, $\mathcal{B} = 1.5$, $\eta = 3.92$, $\tau = 0.1$, $c = 0.3$, $d = 2.2$, $l_1 = 0.2$ and $l_2 = -0.75$: (**a**) A 3D depiction of anti-kink soliton, (**b**) a 2D illustration of anti-kink soliton, and (**c**) contour demonstration of anti-kink soliton.

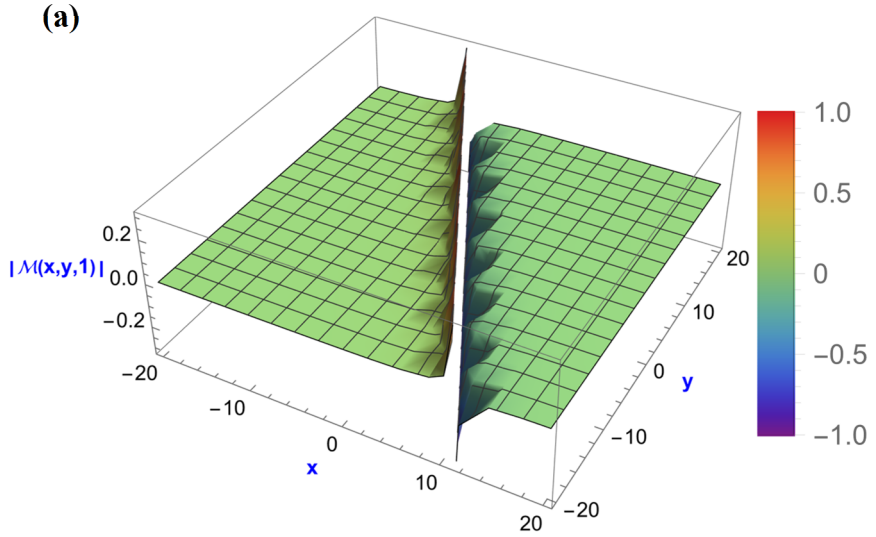

Figure 7. *Cont.*

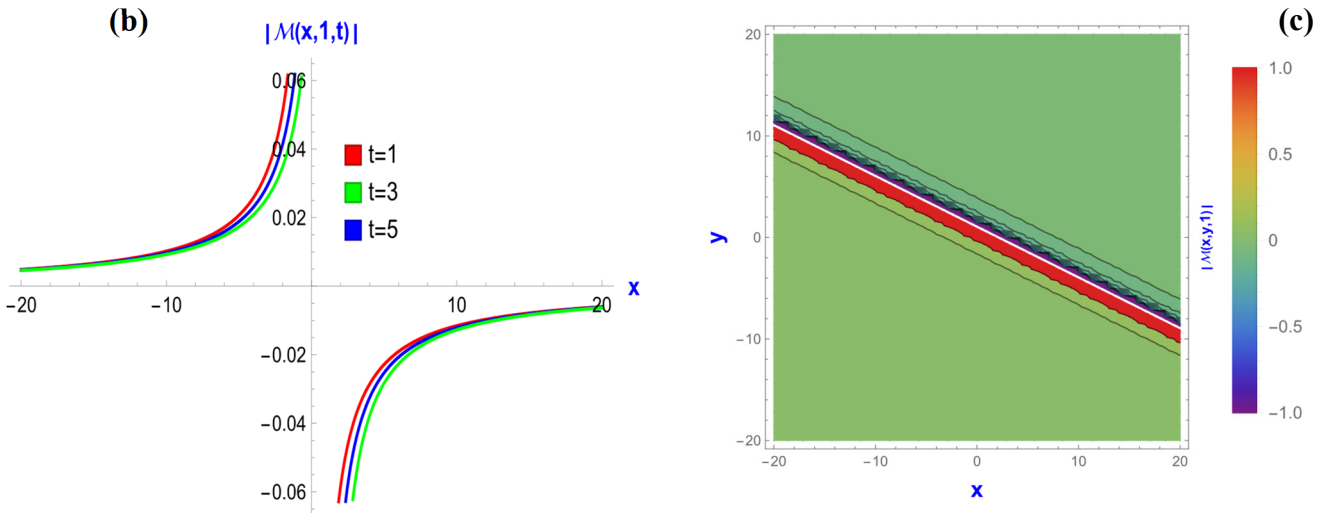

Figure 7. Graphical representations of the solutions $|\mathcal{M}(x,y,t)|$ of Equation (43) for K $= -0.02$, $\mathcal{B} = 1.1, \tau = 0.1$, $n = 1$, $\eta = -0.2$, $c = -0.2$, $d = -0.04$, $l_1 = 5.0$ and $l_2 = 0.2$**:** (**a**) A 3D depiction of dark soliton (**b**) A 2D illustration of dark soliton and (**c**) Contour demonstration of dark soliton.

5.4. Sensitivity Analysis

Similarly, we performed a sensitivity analysis on our derived solution for each scenario of $\lambda = 0$, $\lambda < 0$, and $\lambda > 0$ for the power law nonlinearity of BME. In Figure 8a, we depict the sensitivity of each parameter in Equation (36) for Scenario I. Notably, parameters (λ, c, d, η, τ, K) display negative sensitivity, with λ showing particularly high negative sensitivity. Conversely, the remaining parameters ($\mathcal{B}$, l_1, l_2) exhibit positive sensitivity, albeit not as pronounced as λ. Moreover, l_1 demonstrates almost negligible sensitivity compared to others. For Scenario II ($\lambda < 0$), the results remain largely consistent, with a notable difference: the parameter c, d shows positive sensitivity, as depicted in Figure 8b. In the case of a rational solution ($\lambda = 0$), the most sensitive parameters are c and τ, but they exhibit opposite directions of sensitivity, whereas other parameters are nearly negligible, as illustrated in Figure 8c, which is similar to the Kerr law nonlinearity of BME sensitivity.

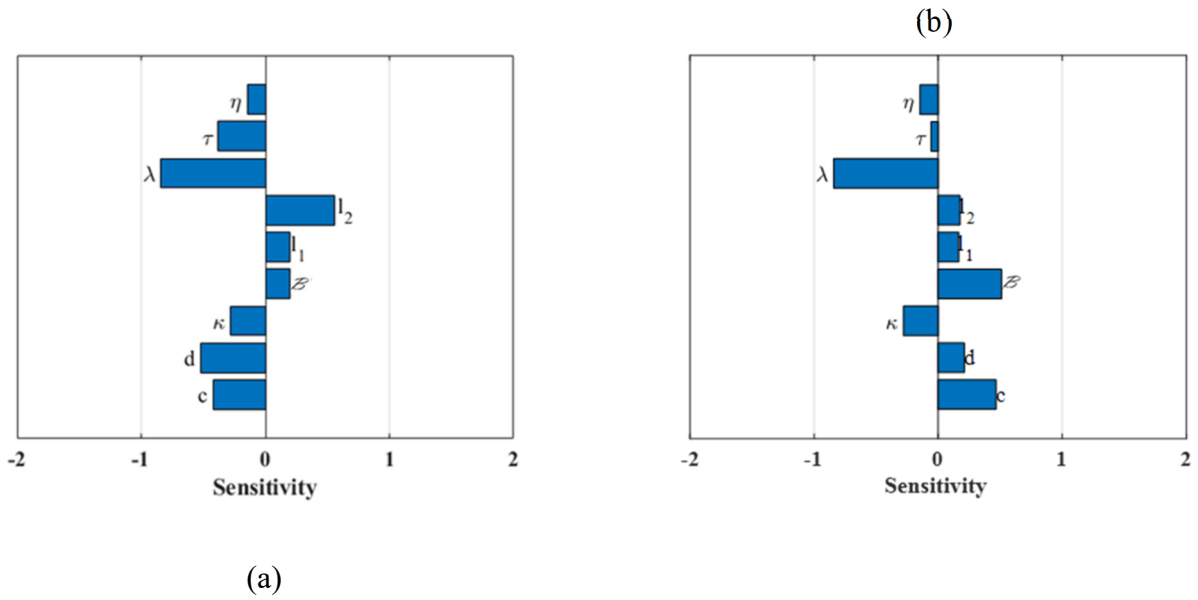

Figure 8. *Cont.*

(c)

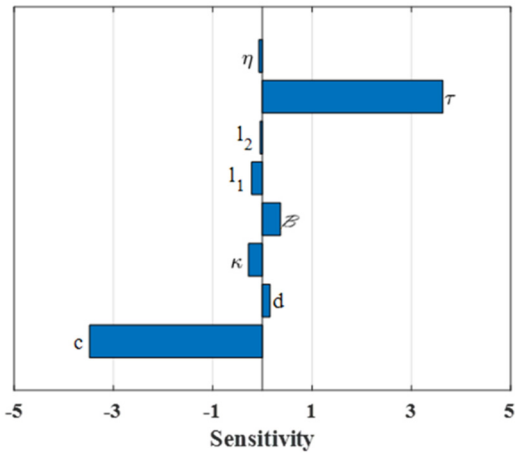

Figure 8. Sensitivity analysis:(**a**) $\lambda > 0$ for Equation (36), (**b**) $\lambda < 0$ for Equation (40), and (**c**) $\lambda = 0$, for Equation (43).

6. Conclusions

The $(G'/G, 1/G)$ method was applied, and several precise optical soliton solutions were obtained for the Kerr and power law nonlinearities of BME. We used an analytical approach to generate several types of nonlinear wave patterns inside these nonlinearities, and different exact solutions in rational, hyperbolic, and trigonometric forms were revealed. Additionally, a sensitivity analysis was conducted to identify parameters that were more sensitive in both the negative and positive senses. The analysis underscores the profound influence of parameters λ, τ, c, $\mathcal{B}$, and K on the precise solutions derived across both Kerr law and power law nonlinearities within the context of BME. Notably, parameter λ emerges as particularly critical across all scenarios, exhibiting heightened sensitivity. Moreover, parameters τ and c demonstrate heightened sensitivity specifically within scenario III. These findings underscore the pivotal role of these parameters in shaping the outcomes of the studied phenomena, offering valuable insights into the nuanced interplay of resultant solutions. Validation through Mathematica software 14 ensured precision, while dynamic visual representations illustrated soliton solutions exhibiting different patterns, including bright solitons, dark solitons, singular solitons, king solitons, anti-kink, and parabolic types. These soliton solutions offer advantages such as energy localization, propagation stability, predictable interactions, precision in optical switching, applications in waveguide design, exploration of nonlinear optical effects, imaging precision, reduced intensity fluctuations, and suitability for optical signal processing in optical physics. The outcomes of this study are novel and hold promise for various forms of BME and related research in optical physics. Moreover, the demonstrated effectiveness and robustness of the applied method in obtaining diverse solitons within different forms of BME further underscore its significance.

Author Contributions: Conceptualization, M.N.H., M.M.M. and M.K.; methodology, M.N.H. and F.A.; software, M.M.M. and M.K.; validation, M.N.H. and F.A.; formal analysis, M.M.M. and M.K.; investigation, M.N.H. and F.A.; writing—original draft preparation, M.N.H. and F.A.; writing—review and editing, M.K. and M.M.M.; visualization, M.M.M.; supervision, M.M.M. and M.K. All authors have read and agreed to the published version of the manuscript.

Funding: This research received no external funding.

Institutional Review Board Statement: I hereby declare that this manuscript is the result of my independent creation under the reviewers' comments. Except for the quoted contents, this manuscript does not contain any research achievements that have been published or written by other individuals or groups.

Data Availability Statement: All data generated or analyzed during this study are included in this article.

Conflicts of Interest: The authors declare no conflicts of interest.

References

1. Verma, P.; Pandit, S.; Kumar, M.; Kumar, V.; Poonam, P. Time-fractional (2 + 1)-dimensional navier-stokes equations: Similarity reduction and exact solutions for one-parameter lie group of rotations. *Phys. Scr.* **2023**, *98*, 075233. [CrossRef]
2. Hossain, M.N.; Miah, M.M.; Hamid, A.; Osman, G.M.S. Discovering new abundant optical solutions for the resonant nonlinear Schrödinger equation using an analytical technique. *Opt. Quantum Electron.* **2024**, *56*, 847. [CrossRef]
3. Kumar, V.; Jiwari, R.; Djurayevich, A.R.; Khudoyberganov, M.U. Hyperbolic (2+1)-dimensional Schrödinger equation: Similarity analysis, Optimal system and complexitons for the one-parameter group of rotations. *Commun. Nonlinear Sci. Numer. Simul.* **2022**, *115*, 106784. [CrossRef]
4. Borhan, J.R.M.; Ganie, A.H.; Miah, M.M.; Iqbal, M.A.; Seadawy, A.R.; Mishra, N.K. A highly effective analytical approach to innovate the novel closed form soliton solutions of the Kadomtsev–Petviashivili equations with applications. *Opt. Quantum Electron.* **2024**, *56*, 938. [CrossRef]
5. Altun, S.; Ozisik, M.; Secer, A.; Bayram, M. Optical solitons for Biswas–Milovic equation using the new Kudryashov's scheme. *Opt.-Int. J. Light Electron Opt.* **2022**, *270*. [CrossRef]
6. Ozdemir, N. Optical solitons for the Biswas-Milovic equation with anti-cubic law nonlinearity in the presence of spatio-temporal dispersion. *Phys. Scr.* **2023**, *98*, 085229. [CrossRef]
7. Iqbal, M.A.; Miah, M.M.; Rasid, M.M.; Alshehri, H.M.; Osman, M.S. An investigation of two integro-differential KP hierarchy equations to find out closed form solitons in mathematical physics. *Arab J. Basic Appl. Sci.* **2023**, *30*, 535–545. [CrossRef]
8. Mia, R.; Mamun Miah, M.; Osman, M.S. A new implementation of a novel analytical method for finding the analytical solutions of the (2+1)-dimensional KP-BBM equation. *Heliyon* **2023**, *9*, e15690. [CrossRef]
9. Yasin, S.; Khan, A.; Ahmad, S.; Osman, M.S. New exact solutions of (3+1)-dimensional modified KdV-Zakharov-Kuznetsov equation by Sardar-subequation method. *Opt. Quantum Electron.* **2024**, *56*, 90. [CrossRef]
10. Rehman, H.U.; Iqbal, I.; Subhi Aiadi, S.; Mlaiki, N.; Saleem, M.S. Soliton Solutions of Klein–Fock–Gordon Equation Using Sardar Subequation Method. *Mathematics* **2022**, *10*, 3377. [CrossRef]
11. Yomba, E. The general projective riccati equations method and exact solutions for a class of nonlinear partial differential equations. *Chin. J. Phys.* **2005**, *43*, 991–1003.
12. Elsayed, M.E.Z.; Khaled, A.E.A. The generalized projective Riccati equations method and its applications for solving two nonlinear PDEs describing microtubules. *Int. J. Phys. Sci.* **2015**, *10*, 391–402. [CrossRef]
13. Chen, W.; Wang, Y.; Tian, L. Lump solution and interaction solutions to the fourth-order extended (2+1)-dimensional Boiti–Leon–Manna–Pempinelli equation. *Commun. Theor. Phys.* **2023**, *75*, 105003. [CrossRef]
14. Kumar, D.; Nuruzzaman, M.; Paul, G.C.; Hoque, A. Novel localized waves and interaction solutions for a dimensionally reduced (2+1)-dimensional Boussinesq equation from N-soliton solutions. *Nonlinear Dyn.* **2022**, *107*, 2717–2743. [CrossRef]
15. Jafari, H.; Kadkhoda, N.; Baleanu, D. Fractional Lie group method of the time-fractional Boussinesq equation. *Nonlinear Dyn.* **2015**, *81*, 1569–1574. [CrossRef]
16. Buckwar, E.; Luchko, Y. Invariance of a Partial Differential Equation of Fractional Order under the Lie Group of Scaling Transformations. *J. Math. Anal. Appl.* **1998**, *227*, 81–97. [CrossRef]
17. Mohanty, S.K.; Kravchenko, O.V.; Deka, M.K.; Dev, A.N.; Churikov, D.V. The exact solutions of the 2+1–dimensional Kadomtsev–Petviashvili equation with variable coefficients by extended generalized [Formula presented]-expansion method. *J. King Saud Univ.-Sci.* **2023**, *35*, 102358. [CrossRef]
18. Naher, H.; Abdullah, F.A. The Basic (G'/G)-Expansion Method for the Fourth Order Boussinesq Equation. *Appl. Math.* **2012**, *03*, 1144–1152. [CrossRef]
19. Zafar, A.; Raheel, M.; Ali, K.K.; Razzaq, W. On optical soliton solutions of new Hamiltonian amplitude equation via Jacobi elliptic functions. *Eur. Phys. J. Plus* **2020**, *135*, 674. [CrossRef]
20. Wen, X.; Lü, D. Extended Jacobi elliptic function expansion method and its application to nonlinear evolution equation. *Chaos Solitons Fractals* **2009**, *41*, 1454–1458. [CrossRef]
21. Babajanov, B.; Abdikarimov, F. The Application of the Functional Variable Method for Solving the Loaded Non-linear Evaluation Equations. *Front. Appl. Math. Stat.* **2022**, *8*, 912674. [CrossRef]
22. Bekir, A.; San, S. The Functional Variable Method to Some Complex Nonlinear Evolution Equations. *J. Mod. Math. Front. Sept* **2012**, *1*, 5–9.
23. Wang, M.; Zhou, Y.; Li, Z. Application of a homogeneous balance method to exact solutions of nonlinear equations in mathematical physics. *Phys. Lett. Sect. A Gen. At. Solid State Phys.* **1996**, *216*, 67–75. [CrossRef]
24. Fan, E.; Zhang, H. A note on the homogeneous balance method. *Phys. Lett. Sect. A Gen. At. Solid State Phys.* **1998**, *246*, 403–406. [CrossRef]
25. Ma, W.X. N-soliton solutions and the Hirota conditions in (1+1)-dimensions. *De Gruyter* **2021**, 1–11. [CrossRef]
26. Ma, W.X. N-soliton solutions and the Hirota conditions in (2+1)-dimensions. *Opt. Quantum Electron.* **2020**, *52*, 511. [CrossRef]

27. Islam, S.M.R.; Arafat, S.M.Y.; Wang, H. Abundant closed-form wave solutions to the simplified modified Camassa-Holm equation. *J. Ocean Eng. Sci.* **2023**, *8*, 238–245. [CrossRef]
28. Zhang, Z.Y. Exact traveling wave solutions of the perturbed Klein-Gordon equation with quadratic nonlinearity in (1+1)-dimension, Part I: Without local inductance and dissipation effect. *Turk. J. Phys.* **2013**, *37*, 259–267. [CrossRef]
29. Kumar, D.; Paul, G.C.; Seadawy, A.R.; Darvishi, M.T.J. A variety of novel closed-form soliton solutions to the family of Boussinesq-like equations with different types. *Ocean Eng. Sci.* **2022**, *7*, 543–554. [CrossRef]
30. Parkes, E.J.; Duffy, B.R. An automated tanh-function method for finding solitary wave solutions to non-linear evolution equations. *Comput. Phys. Commun.* **1996**, *98*, 288–300. [CrossRef]
31. Fan, E. Extended tanh-function method and its applications to nonlinear equations. *Phys. Lett. A* **2000**, *277*, 212–218. [CrossRef]
32. Kumar, A.; Pankaj, R.D. Tanh–coth scheme for traveling wave solutions for Nonlinear Wave Interaction model. *J. Egypt. Math. Soc.* **2015**, *23*, 282–285. [CrossRef]
33. Mamun, A.-A.-; Ananna, S.N.; An, T.; Asaduzzaman, M.; Miah, M.M. Solitary wave structures of a family of 3D fractional WBBM equation via the tanh–coth approach. *Partial Differ. Equ. Appl. Math.* **2022**, *5*, 100237. [CrossRef]
34. Habib, M.A.; Ali, H.M.S.; Miah, M.M.; Akbar, M.A. The generalized Kudryashov method for new closed form traveling wave solutions to some NLEEs. *AIMS Math.* **2019**, *4*, 896–909. [CrossRef]
35. Islam, S.; Khan, K.; Arnous, A.H. Generalized Kudryashov method for solving some. *New Trends Math. Sci.* **2015**, *57*, 46–57.
36. Raza, N.; Aslam, M.R.; Rezazadeh, H. Analytical study of resonant optical solitons with variable coefficients in Kerr and non-Kerr law media. *Opt. Quantum Electron.* **2019**, *51*, 59. [CrossRef]
37. Roshid, H.O.; Kabir, M.R.; Bhowmik, R.C.; Datta, B.K. Investigation of Solitary wave solutions for Vakhnenko-Parkes equation via exp-function and Exp($-\phi(\xi)$)-expansion method. *Springerplus* **2014**, *3*, 692. [CrossRef]
38. Fokas, A.S.; Lenells, J. The unified method: I. Nonlinearizable problems on the half-line. *J. Phys. A Math. Theor.* **2012**, *45*, 195201. [CrossRef]
39. Abdel-Gawad, H.I.; Osman, M. On shallow water waves in a medium with time-dependent dispersion and nonlinearity coefficients. *J. Adv. Res.* **2015**, *6*, 593–599. [CrossRef]
40. Ma, W.X.; Huang, T.; Zhang, Y. A multiple exp-function method for nonlinear differential equations and its application. *Phys. Scr.* **2010**, *82*, 065003. [CrossRef]
41. Ma, W.X.; Zhu, Z. Solving the (3 + 1)-dimensional generalized KP and BKP equations by the multiple exp-function algorithm. *Appl. Math. Comput.* **2012**, *218*, 11871–11879. [CrossRef]
42. Sadaf, M.; Arshed, S.; Ghazala Akram, I. Exact soliton and solitary wave solutions to the Fokas system using two variables (G′/G,1/G)-expansion technique and generalized projective Riccati equation method. *Opt.-Int. J. Light Electron. Opt.* **2022**, *268*, 169713. [CrossRef]
43. Miah, M.M.; Ali, H.M.S.; Akbar, M.A.; Wazwaz, A.M. Some applications of the (G′/G, 1/G)-expansion method to find new exact solutions of NLEEs. *Eur. Phys. J. Plus* **2017**, *132*, 252. [CrossRef]
44. Vivas-Cortez, M.; Akram, G.; Sadaf, M.; Arshed, S.; Rehan, K.; Farooq, K. Traveling wave behavior of new (2+1)-dimensional combined KdV–mKdV equation. *Results Phys.* **2023**, *45*, 106244. [CrossRef]
45. Inan, I.E.; Ugurlu, Y. New Applications of the (G′/G, 1/G)-Expansion Method. *Acta Phys. Pol. A* **2015**, *128*, 245–251. [CrossRef]
46. Zayed, E.M.E.; Alurrfi, K.A.E. The (G′/G, 1/G)-Expansion Method and Its Applications for Solving Two Higher Order Nonlinear Evolution Equations. *Math. Probl. Eng.* **2014**, *2014*, 746538. [CrossRef]
47. Sirisubtawee, S.; Koonprasert, S.; Sungnul, S. Some applications of the (G′/G, 1/G)-expansion method for finding exact traveling wave solutions of nonlinear fractional evolution equations. *Symmetry* **2019**, *11*, 952. [CrossRef]
48. Miah, M.M.; Seadawy, A.R.; Ali, H.M.S.; Akbar, M.A. Abundant closed form wave solutions to some nonlinear evolution equations in mathematical physics. *J. Ocean Eng. Sci.* **2020**, *5*, 269–278. [CrossRef]
49. Rasid, M.M.; Miah, M.M.; Ganie, A.H.; Alshehri, H.M.; Osman, M.S.; Ma, W.X. Further advanced investigation of the complex Hirota-dynamical model to extract soliton solutions. *Mod. Phys. Lett. B* **2023**, *38*, 2450074. [CrossRef]
50. Li, L.X.; Li, E.Q.; Wang, M.L. The (G′/G, 1/G)-expansion method and its application to travelling wave solutions of the Zakharov equations. *Appl. Math.* **2010**, *25*, 454–462. [CrossRef]
51. Hossain, M.N.; Miah, M.M.; Duraihem, F.Z.; Rehman, S. Stability, modulation instability, and analytical study of the confirmable time fractional Westervelt equation and the Wazwaz Kaur Boussinesq equation. *Opt. Quantum Electron.* **2024**, *56*, 948. [CrossRef]
52. Biswas, A. Quasi-stationary optical solitons with dual-power law nonlinearity. *Opt. Commun.* **2004**, *235*, 183–194. [CrossRef]
53. Zhou, Q.; Ekici, M.; Sonmezoglu, A.; Mirzazadeh, M.; Eslami, M. Optical solitons with Biswas–Milovic equation by extended trial equation method. *Nonlinear Dyn.* **2016**, *84*, 1883–1900. [CrossRef]
54. Ali, A.; Ahmad, J.; Javed, S. Exploring the dynamic nature of soliton solutions to the fractional coupled nonlinear Schrödinger model with their sensitivity analysis. *Opt. Quantum Electron.* **2023**, *55*, 810. [CrossRef]
55. Chahlaoui, Y.; Ali, A.; Ahmad, J.; Hussain, R.; Javed, S. Dynamical behavior of optical soliton solutions, time series and sensitivity analysis to the Schrödinger model with eta fractional derivative. *Opt. Quantum Electron.* **2024**, *56*, 704. [CrossRef]